Available online at www.elixirpublishers.com (Elixir International Journal)

Applied Mathematics

Elixir Appl. Math. 41 (2011) 5592-5603

ISSN: 2229-712X

Numerical modelling of transient dissipative radiation free convection heat and mass transfer from a non-isothermal cone with variable surface conditions

V.Ramachandra Prasad[1], B.Vasu[1] and O.Anwar beg[2]

[1]Department of Mathematics, Madanapalle Institute of Technology and Science, Madanapalle-517325, India.

[2]Engineering Magnetohydrodynamics, Energy Systems and Heat Transfer Research, Mechanical Engineering Program, Sheaf Building, Sheffield Hallam University, Sheffield, S1 1WB, UK, England, UK.

ARTICLE INFO

Article history:

Received: 10 September 2011;

Received in revised form:

15 November 2011;

Accepted: 25 November 2011;

Keywords

Unsteady Flow,
Heat and Mass Transfer, Cone,
Variable surface temperature and concentration,
Viscous dissipation,
Thermal radiation,
Finite difference method,
Eckert number,
Buoyancy.

ABSTRACT

The combined effects of thermal radiation and viscous dissipation on unsteady, laminar, free convective flow with heat and mass transfer over an incompressible viscous fluid past a non-isothermal vertical cone with variable surface temperature and concentration are considered in this article. The dimensionless governing equations of the flow that are unsteady, coupled and non-linear partial differential equations are solved by an efficient, accurate and unconditionally stable finite difference scheme of Crank-Nicolson type. The velocity, temperature and concentration fields have been studied for the effect of Eckert number (Ec), Prandtl number (Pr), radiation parameter (F), Schmidt number (Sc), buoyancy ratio parameter (N), semi vertical cone angle (ϕ), surface temperature power law exponent (n) and surface concentration power law exponent (m). The local skin-friction, Nusselt number and Sherwood number are also presented and analyzed graphically. It is observed that, when the radiation parameter increases, the velocity decreases close to the cone surface and an increase in Eckert number is observed to increase both velocity and temperature. The present results are compared with the available results in literature and are found to be in good agreement.

Introduction

Numerical modeling of combined heat and mass transfer flows is important in many industrial applications including geothermal energy, solar energy systems, biomechanics, rocket propulsion, electronic circuit systems, metallurgical processing, chemical engineering transport phenomena and air-conditioning systems. Extensive studies have been reported in all these areas employing a wide variety of numerical simulation methods including finite elements, finite differences, network simulation and CFD (Computational Fluid Dynamics). Frequently external free convection boundary layer flows from simple geometries such as flat plates, wedges, spheres, ellipses and cylinders have been examined in the literature. An extensive review of these works is documented in Gebhart et al [13]. Transport processes have also been studied for the special geometry of a *vertical cone* which finds important applications in chemical processing operations [25] and also rocket nose thermophysical simulation [28]. Initial studies have dwelled on purely thermal convection flows only. Hering and Grosh [22] showed that the similarity solutions also exist when the surface temperature of the cone is a power function of the distance along a cone ray. Gorla and Stratman [17] discussed the effects of the transverse curvature on the free convection flow past a slender vertical cone. Pop and Takhar [32] made an interesting study of the laminar compressible natural convection about a vertical cone, showing that compressibility increases the heat transfer rate at the wall for small values of the wall-ambient temperature difference parameter. Hasan and Majumdar [20] studied the combined heat and masstransfer characteristics under mixed convective flow along the external surface of a vertical circular cone for cones with large apex angles whereby the radial curvature effects are negligible. They considered both buoyancy-aided and opposing flows for the diffusion of common gases and vapors in air. Yih [39] studied numerically the free convection heat and mass transfer from truncated cone embedded in a saturated porous medium subjected with thermal and mass diffusion using the Keller box implicit difference method. He showed that both local Nusselt number and local Sherwood number increase with increasing buoyancy effects and increase and decrease respectively with decreasing Lewis number. Cheng [10] used the cubic spline collocation method to analyze the free convection heat and mass transfer from a wavy conical body embedded in a porous medium. Elperin and Fominykh [11] studied combined heat and mass transfer from a cone to a non-Newtonian fluid when the concentration level of the solute in the solvent is finite (finite dilution of solute approximation). They showed that mass transfer rate increases with solute concentration level. These studies did not consider the presence of viscous heating (dissipation) which can be significant in aerosol deposition processes [16], micro-rockets [30], polymer injection moulding [21], microchannel systems [31] etc. The effect of viscous dissipation on natural convection has been studied by Gebhart [14] for a power-law vertical wall variation. He obtained a perturbation solution in terms of a parameter which could not be expressed in terms of the Rayleigh number or the Prandtl number, and observed its increasing effect as the Prandtl number increases. Later Gebhart and Mollendorf [15] obtained the similarity solution for the same problem when exponential wall temperature variation is used and a similar trend was observed.

Tele:

E-mail addresses: rcpmaths@mits.ac.in, bvsmaths1@gmail.com

Rajasekaran and Palekar [34] studied the influence of Eckert number on rotating mixed convection using Merk's series expansions. Mahajan and Gebhart [27] reported on the influence of viscous heating dissipation effects in natural convection flows. Bég*et al.* [4] studied the influence of vorticity diffusion and viscous dissipation on thermoconvection flow in a non-Darcian porous medium. Bég*et al.* [5] later investigated with finite elements the viscous dissipation effects in viscoelastic convection flow in a porous regime. Bég*et al* [6] have also studied dissipation effects in biomagnetic heat transfer in porous media, showing that Eckert number has a significant effect on temperature distributions. These studies did not consider *thermal radiation* effects which attain significance in high temperature systems including blast furnace processes, glass manufacture, solar energy collector systems [23] and environmental hazards such as accidental radiation releases [36]. In simulating thermal radiation processes which are coupled with other modes e.g. convection, conduction, frequently highly nonlinear differential equations arise. To circumvent solution of such systems an algebraic or flux approximation is often employed. Numerous methodologies have been developed including the Rosseland diffusion approximation, Milne-Eddington approximation, Discrete Ordinates method, P-N differential approximation methods etc. An excellent summary of these approaches is available in Modest [29]. Numerical analysis of thermal convection flows coupled with thermal radiation has received extensive attention. Behnia*et al* [7] used a two-band radiative transfer model and a finite difference technique to study combined natural convection and radiation in a rectangular, two-dimensional cavity containing a non-participating (i.e. transparent) fluid over an extensive range of Rayleigh numbers. Engelman and Jamnia [12] used the FIDAP computational fluid dynamics solver to simulate the effects of grey-diffuse surface radiation on the temperature field of fluid flows in a non-participating medium. They decoupled the energy and radiation exchange equations and used a macro surface model containing a number of radiating boundary surfaces to convey information from the radiating boundary into the fluid regime. Weng and Chu [38] used the P-1 differential spherical harmonics approximation to analyze the composite free convection and radiation in a vertical annulus. Bég*et al* [2] studied the optically-thick steady radiative-convection boundary layer flow using the Rossleand diffusion flux approximation and a numerical shooting method. Banda *et al* [1] used the lattice-Boltzmann method to simulate incompressible convection-radiation flows in two-dimensional enclosures with a discrete-ordinates radiative formulation and a non-oscillatory relaxation scheme to solve the coupled moment equations. Bég*et al* [3] used the network simulation thermodynamic numerical method to analyze unsteady free convective-radiative heat and mass transfer in optically-thick saturated porous media. Combined dissipation and thermal radiation effects on free convection flows have also been studied in the literature. Takhar*et al* [37] used the Cogley-Vinceti-Giles differential approximation to study coupled non-gray convection-radiation boundary layers in a porous medium using the Keller Box finite difference method. They showed that flow is decelerated in the boundary layer with increasing thermal radiation flux whereas surface heat transfer gradients are strongly enhanced. Viscous heating (as simulated via the Eckert number, Ec) was also shown to boost shear stresses for positive Ec but to decelerate the flow for negative Ec. Conversely heat transfer gradients were shown to be increased with negative Ec values but depressed with positive Ec values. Chamkha*et al* [9] used the Rosseland diffusion flux model to analyze the buoyancy-driven dissipative natural convection-radiation boundary layer flow from a wedge in a porous medium. They showed that an increase in Boltzmann-Rosseland radiation-conduction number and negative Eckert number enhances heat transfer gradients at the wedge face considerably. In the present study we analyze numerically the transient radiation-convection heat and mass transfer from a vertical cone with significant viscous dissipation and thermal radiation effects. Such a study has immediate applications in chemical process engineering and has to the authors' knowledge not appeared thusfar in the scientific literature. A well-tested, numerically stable Crank-Nicolson finite difference procedure is employed.

Mathematical Model

Consider the axi-symmetric unsteady laminar free convection heat and mass transfer in a viscous, incompressible, absorbing-emitting, non-scattering, optically-thick gas from a non-isothermal vertical cone with variable surface temperature and concentration in the presence of thermal radiation and viscous dissipation. Initially, it is assumed that the cone surface and the surrounding fluid which are at rest possess the same temperature T'_∞ and concentration level C'_∞ everywhere in the fluid. At time $t' > 0$, the temperature of the cone surface and the concentration near the cone surface are elevated to $T' = T'_\infty + ax^n, C' = C'_\infty + ax^m$ respectively, and are sustained as constant thereafter. The concentration C' of the diffusing species in the binary mixture is assumed to be very less in comparison to the other chemical species, which are present. This leads to the assumption that the Soret and Dufour effects are negligible. The co-ordinate system chosen (as shown in Fig.1) is such that the *x*- coordinate is directed along the surface of the cone from the apex (x = 0) and the *y*- coordinate is orientated perpendicular to this i.e. at right angles to the cone surface, outwards. Here, ϕ designates the semi-vertical angle of the cone and *r* is the local radius of the cone. In compliance with the Boussinesq approximation, all fluid properties are assumed constant except for density variations, which induce *buoyancy* forces, these contributing a dominant, driving role in the free convection regime.

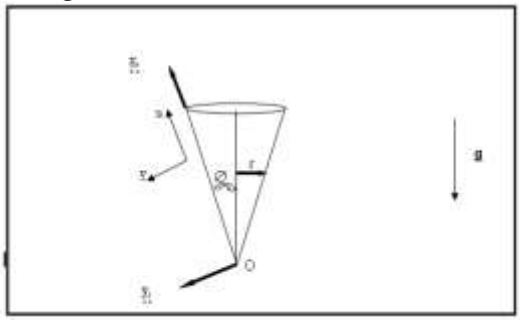

Figure 1: Physical Model

Then under the above assumptions, the governing boundary layer equations of mass, momentum, energy and species concentration for free convective flows with Boussinesq's approximation are as follows.

$$\frac{\partial (ur)}{\partial x} + \frac{\partial (vr)}{\partial y} = 0 \qquad (1)$$

$$\frac{\partial u}{\partial t'}+u\frac{\partial u}{\partial x}+v\frac{\partial u}{\partial y}=\nu\frac{\partial^2 u}{\partial y^2}+g\beta\cos\phi(T'-T'_\infty)+g\beta^*\cos\phi(C'-C'_\infty) \tag{2}$$

$$\frac{\partial T'}{\partial t'}+u\frac{\partial T'}{\partial x}+v\frac{\partial T'}{\partial y}=\alpha\frac{\partial^2 T'}{\partial y^2}-\frac{1}{\rho c_p}\frac{\partial q_r}{\partial y}+\frac{\nu}{c_p}\left(\frac{\partial u}{\partial y}\right)^2 \tag{3}$$

$$\frac{\partial C'}{\partial t'}+u\frac{\partial C'}{\partial x}+v\frac{\partial C'}{\partial y}=D\frac{\partial^2 C'}{\partial y^2} \tag{4}$$

The initial and boundary conditions are prescribed as:

$$t'\le 0: u=0, v=0, T'=T'_\infty, C'=C'_\infty$$

for all x, y,

$$t'>0: u=0, v=0, T'=T'_\infty+ax^n, C'=C'_\infty+ax^m$$

at y = 0,

$$u=0, T'=T'_\infty, C'=C'_\infty \text{ at } x=0,$$

$$u\to 0, T'\to T'_\infty, C'\to C'_\infty \quad \text{as } y\to\infty. \tag{5}$$

Employing the Rosseland diffusion approximation [29], leads to the following expression for radiative heat flux q_r in the energy conservation Eqn. 3:

$$q_r=-\frac{4\sigma_s}{3k_e}\frac{\partial T'^4}{\partial y} \tag{6}$$

where σ_s is the Stefan-Boltzmann constant and k_e is the mean absorption coefficient, respectively. It should be noted that by using the Rosseland approximation we limit our analysis to *optically thick* fluids. Refractive index of the gas medium is constant. Unidirectional radiation flux, Q_r, is considered and it is assumed that $\frac{\partial q_r}{\partial y} >> \frac{\partial q_r}{\partial x}$. This model is valid for optically-thick media in which thermal radiation propagates only a limited distance prior to experiencing scattering or absorption. The local thermal radiation intensity is due to radiation emanating from proximate locations in the vicinity of which emission and scattering are comparable to the location of interest. For zones where conditions are appreciably different thermal radiation has been shown to be greatly attenuated before arriving at the location under consideration as discussed by Behnia*et al.* [7]. The energy transfer depends on conditions only in the area adjacent to the plate regime i.e. the boundary layer regime. Rosseland's model yields accurate results for intensive absorption i.e. *optically-thick flows* which are optically far from the bounding surface. Implicit in this approximation is also the existence of wavelength regions where the optical thickness may exceed a value of five. As such the Rosseland model, while limited compared with other flux models, can simulate to a reasonable degree of accuracy thermal radiation in problems ranging from thermal radiation transport via gases at low density to thermal radiation simulations associated with nuclear blast waves. If temperature differences within the flow are sufficiently small, then Eq. (6) can be linearized by expanding T'^4 into the Taylor series about T'_∞, which after neglecting higher order terms takes the form:

$$T'^4\cong 4T'^3_\infty T'-3T'^4_\infty \tag{7}$$

In view of Eqs. (6) and (7), Eq. (3) reduces to:

$$\frac{\partial T'}{\partial t'}+u\frac{\partial T'}{\partial x}+v\frac{\partial T'}{\partial y}=\alpha\frac{\partial^2 T'}{\partial y^2}+\frac{16\sigma_s T'^3_\infty}{3k_e\rho c_p}\frac{\partial^2 T'}{\partial y^2}+\frac{\nu}{c_p}\left(\frac{\partial u}{\partial y}\right)^2 \tag{8}$$

where all parameters are defined in the nomenclature. Local skin-friction (wall shear stress), local Nusselt number (surface heat transfer gradient) and local Sherwood number (surface species transfer gradient) are given respectively by:

$$\tau_x=-\mu\left(\frac{\partial u}{\partial y}\right)_{y=0} \tag{9}$$

$$Nu_x=\frac{-x\left(\frac{\partial T'}{\partial y}\right)_{y=0}}{T'_w-T'_\infty} \tag{10}$$

$$Sh_x=\frac{-x\left(\frac{\partial C'}{\partial y}\right)_{y=0}}{C'_w-C'_\infty} \tag{11}$$

Proceeding with analysis, we implement the following non-dimensional quantities to facilitate a numerical solution to the boundary value problem defined by Eqns. (1) to (4) under conditions (5) :

$$X=\frac{x}{L},\ Y=\frac{y}{L}(Gr_L)^{\frac{1}{4}},\ R=\frac{r}{L}, \text{ where } r=x\sin\phi,$$

$$V=\frac{vL}{\nu}(Gr_L)^{\frac{-1}{4}}, U=\frac{uL}{\nu}(Gr_L)^{\frac{-1}{2}}, t=\frac{\nu t'}{L^2}(Gr_L)^{\frac{1}{2}}, \tag{12}$$

$$T=\frac{T'-T'_\infty}{T'_w(L)-T'_\infty}, Gr_L=\frac{g\beta(T'_w(L)-T'_\infty)L^3}{\nu^2}, \Pr=\frac{\nu}{\alpha},$$

$$F=\frac{k_e k}{4\sigma_s T'^3_\infty}$$

$$C=\frac{C'-C'_\infty}{C'_w-C'_\infty},\ Ec=\frac{U_0^2}{c_p(T'_w-T'_\infty)}, N=\frac{\beta^*(C'_w-C'_\infty)}{\beta(T'_w-T'_\infty)},$$

$$Sc=\frac{\nu}{D}$$

Eqs. (1), (2), (8) and (4) are thereby rendered into the following non-dimensional form:

$$\frac{\partial(UR)}{\partial X}+\frac{\partial(VR)}{\partial Y}=0 \tag{13}$$

$$\frac{\partial U}{\partial t}+U\frac{\partial U}{\partial X}+V\frac{\partial U}{\partial Y}=\frac{\partial^2 U}{\partial Y^2}+T\cos\phi+NC\cos\phi \tag{14}$$

$$\frac{\partial T}{\partial t}+U\frac{\partial T}{\partial X}+V\frac{\partial T}{\partial Y}=\frac{1}{\Pr}\left[1+\frac{4}{3F}\right]\frac{\partial^2 T}{\partial Y^2}+Ec\left(\frac{\partial U}{\partial Y}\right)^2 \tag{15}$$

$$\frac{\partial C}{\partial t}+U\frac{\partial C}{\partial X}+V\frac{\partial C}{\partial Y}=\frac{1}{Sc}\frac{\partial^2 C}{\partial Y^2} \tag{16}$$

The corresponding initial and boundary conditions are:

$$t \le 0 : U = 0, V = 0, T = 0, C = 0 \text{ for all X, Y,}$$
$$t > 0 : U = 0, V = 0, T = X^n, C = X^m \text{ at Y = 0,} \quad (17)$$
$$U = 0,\ T = 0, C = 0 \quad \text{at X = 0,}$$
$$U \to 0, T \to 0,\ C \to 0 \text{ as } Y \to \infty .$$

Here again all parameters have been defined earlier in the nomenclature. The dimensionless local values of the skin friction (surface shear stress), the Nusselt number (surface heat transfer gradient) and the Sherwood number (surface concentration gradient) are computed using the following expressions:

$$\tau_x = -\left(\frac{\partial U}{\partial Y}\right)_{Y=0} \quad (18)$$

$$Nu_x = -X\left(\frac{\partial T}{\partial Y}\right)_{Y=0} \quad (19)$$

$$Sh_x = -X\left(\frac{\partial C}{\partial Y}\right)_{Y=0} \quad (20)$$

Numerical Solution

In order to solve these unsteady, non-linear coupled equations (13) to (16) under the conditions (17), an implicit finite difference scheme of Crank-Nicolson type has been employed. This method has been extensively developed in recent years and remains one of the most reliable procedures for solving partial differential equation systems. It is unconditionally stable. It utilizes a central differencing procedure for space and is an implicit method. The partial differential terms are converted to difference equations and the resulting algebraic problem is solved using a triadiagonal matrix algorithm. For transient problems a trapezoidal rule is utilized and provides second-order convergence. The Crank-Nicolson Method (CNM) scheme has been used in numerous heat transfer, radiation and convection flow problems. Ransom and Fulton [35] discussed a modified, optimized version of the Crank-Nicolson method for general thermal engineering problems. Lin and Huang [26] studied thermal radiation effects on laminar forced convection in thermally developing circular pipe flow using an integral formulation for the divergence of radiative heat flux, a finite element node approximation technique and the Crank-Nicolson finite difference method with an iterative procedure. Hadley [19] used the Crank-Nicolson method with a new boundary condition to study beam propagation emitting radiation with a minimum reflection coefficient, considering both two and three-dimensional cases. Krishnaprakas*et al* [24] used the Chandrasekhar discrete ordinates method and the Crank-Nicolson method to study combined conduction and radiation heat transfer in a gray planar nonlinearly anisotropic scattering medium bounded between two plane parallel surfaces reflecting both diffusely and specularly. Prasad *et al* [33] used Crank-Nicolson scheme to analyze the transient convective heat and mass transfer with thermal radiation effects along a vertical impulsively started plane. Very recently GouseMohiddin*et al* [18] studied the transient natural convection heat and mass transfer in viscoelastic boundary layer flow along a vertical cone using the Crank-Nicolson method. The CNM method has been found to work very efficiently for parabolic type partial differential equations as exemplified by boundary-layer flows The finite difference equations corresponding to equations (13) to (16) are discretized using CNM as follows:

Mass Conservation:

$$\frac{U_{i,j}^{k+1} - U_{i-1,j}^{k+1} + U_{i,j}^{k} - U_{i-1,j}^{k} + U_{i,j-1}^{k+1} - U_{i-1,j-1}^{k+1} + U_{i,j-1}^{k} - U_{i-1,j-1}^{k}}{4\Delta X}$$
$$+ \frac{V_{i,j}^{k+1} - V_{i,j-1}^{k+1} + V_{i,j}^{k} - V_{i,j-1}^{k}}{2\Delta Y} + \frac{U_{i,j}^{k+1} + U_{i,j-1}^{k+1} + U_{i,j}^{k} + U_{i,j-1}^{k}}{4i\Delta X} = 0, \quad (21)$$

Momentum Conservation:

$$\frac{U_{i,j}^{k+1} - U_{i,j}^{k}}{\Delta t} + U_{i,j}^{k}\frac{U_{i,j}^{k+1} - U_{i-1,j}^{k+1} + U_{i,j}^{k} - U_{i-1,j}^{k}}{2\Delta X} + V_{i,j}^{k}\frac{U_{i,j+1}^{k+1} - U_{i,j-1}^{k+1} + U_{i,j+1}^{k} - U_{i,j-1}^{k}}{4\Delta Y}$$
$$= \frac{U_{i,j-1}^{k+1} - 2U_{i,j}^{k+1} + U_{i,j+1}^{k+1} + U_{i,j-1}^{k} - 2U_{i,j}^{k} + U_{i,j+1}^{k}}{2(\Delta Y)^2} + \frac{T_{i,j}^{k+1} + T_{i,j}^{k}}{2}\cos\phi + N\cos\phi\frac{C_{i,j}^{k+1} + C_{i,j}^{k}}{2} \quad (22)$$

Energy (Heat) Conservation

$$\frac{T_{i,j}^{k+1} - T_{i,j}^{k}}{\Delta t} + U_{i,j}^{k}\frac{T_{i,j}^{k+1} - T_{i-1,j}^{k+1} + T_{i,j}^{k} - T_{i-1,j}^{k}}{2\Delta X} + V_{i,j}^{k}\frac{T_{i,j+1}^{k+1} - T_{i,j-1}^{k+1} + T_{i,j+1}^{k} - T_{i,j-1}^{k}}{4\Delta Y}$$
$$= \frac{1}{\Pr}\left(1 + \frac{4}{3F}\right)\frac{T_{i,j-1}^{k+1} - 2T_{i,j}^{k+1} + T_{i,j+1}^{k+1} + T_{i,j-1}^{k} - 2T_{i,j}^{k} + T_{i,j+1}^{k}}{2(\Delta Y)^2} + Ec\left(\frac{U_{i,j+1}^{k} - U_{i,j}^{k}}{\Delta Y}\right)^2 \quad (23)$$

Species (Concentration) Conservation:

$$\frac{C_{i,j}^{k+1} - C_{i,j}^{k}}{\Delta t} + U_{i,j}^{k}\frac{C_{i,j}^{k+1} - C_{i-1,j}^{k+1} + C_{i,j}^{k} - C_{i-1,j}^{k}}{2\Delta X} + V_{i,j}^{k}\frac{C_{i,j+1}^{k+1} - C_{i,j-1}^{k+1} + C_{i,j+1}^{k} - C_{i,j-1}^{k}}{4\Delta Y}$$
$$= \frac{1}{Sc}\frac{C_{i,j-1}^{k+1} - 2C_{i,j}^{k+1} + C_{i,j+1}^{k+1} + C_{i,j-1}^{k} - 2C_{i,j}^{k} + C_{i,j+1}^{k}}{2(\Delta Y)^2} \quad (24)$$

Here the region of integration is considered as a rectangle with $X_{\max} = 1$ and $Y_{\max} = 20$ where $Y_{\max}$ corresponds to $Y = \infty$ which lies well outside both the momentum and thermal boundary layers. The maximum of Y was chosen as 20, after some preliminary numerical experiments such that the last two boundary conditions of (17) were satisfied within the tolerance limit 10^{-5}. The mesh sizes have been fixed as $\Delta X = 0.05$, $\Delta Y = 0.05$ with time step $\Delta t = 0.01$. The computations are executed initially by reducing the spatial mesh sizes by 50% in one direction, and later in both directions by 50%. The results are compared. It is observed that, in all the cases, the results differ only in the fifth decimal place. Hence, the choice of the mesh sizes is verified as extremely efficient. The coefficients of $U_{i,j}^{k}$ and $V_{i,j}^{k}$ appearing in the finite difference equations are treated as constant at any one-time step. Here i designates the grid point along the *X*-direction, j along the *Y*-direction and k in the time variable, *t*. The values of *U, V, T* and *C* are known at all grid points when *t = 0* from the initial conditions.

The computations for *U, V, T* and *C* at a time level (*k + 1*), using the values at previous time level *k* are executed as follows. The finite-difference equation (24) at every internal nodal point on a particular $i-$level constitutes a tri-diagonal system of equations and is solved by the robust Thomas algorithm as discussed in Carnahan *et al.* [8]. Thus, the values of *C* are

known at *every nodal point* at a particular i at (k + 1)th time level. Similarly, the values of *U* and *T* are calculated from equations (22), (23) respectively, and finally the values of *V* are calculated explicitly by using equation (21) at every nodal point on a particular $i-$level at (k + 1)thtime level. In a similar manner, computations are carried out by moving along i-direction. After computing values corresponding to each i at a time level, the values at the next time level are determined in a similar manner. Computations are repeated until the steady state is attained. The steady state solution is assumed to have been reached when the *absolute difference* between the values of the velocity *U*, temperature *T*, as well as concentration *C* at two consecutive time steps are less than 10^{-5} at all grid points. The scheme is unconditionally stable. The local truncation error is $O(\Delta t^2 + \Delta X^2 + \Delta Y^2)$ and it tends to zero as $\Delta t, \Delta X$ and ΔY tend to zero. It follows that the CNM scheme is compatible. Stability and compatibility ensure the convergence.

Results and Discussion

For conservation of space, selective computations have been reproduced here. Default values of the parameters are as follows: Eckert number (*Ec*) = 0.1 (which corresponds to cooling of the cone surface i.e. conduction of heat away from the cone into the surrounding gas regime), buoyancy ratio parameter (*N*) = 1.0, Schmidt number (*Sc*) = 0.6 (oxygen diffusing in the primary fluid i.e. air), Prandtl number (*Pr*) = 0.7 (air), semi-vertical angle of the cone (ϕ) = 20^0, radiation parameter (*F*) = 3.0 (strong thermal radiation compared with thermal conduction), surface temperature power law exponent (*n*) = 0.5 and surface concentration power law exponent (*m*) = 0.5. All graphs therefore correspond to these values unless otherwise indicated.

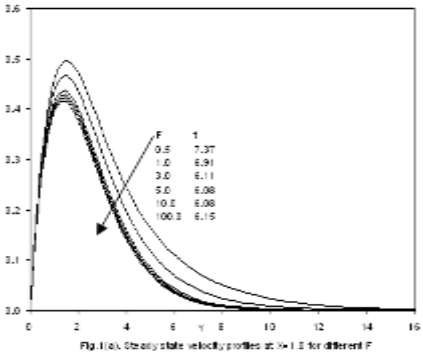

Fig.1(a). Steady state velocity profiles at X=1.0 for different F

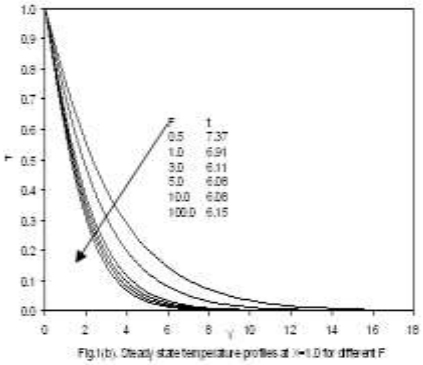

Fig.1(b). Steady state temperature profiles at X=1.0 for different F

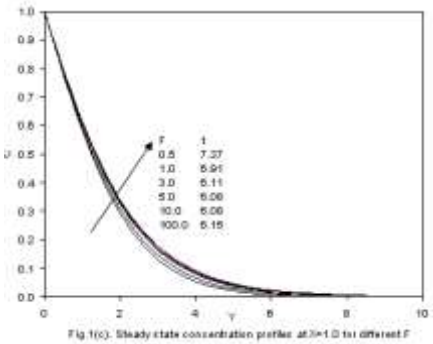

Fig.1(c). Steady state concentration profiles at X=1.0 for different F

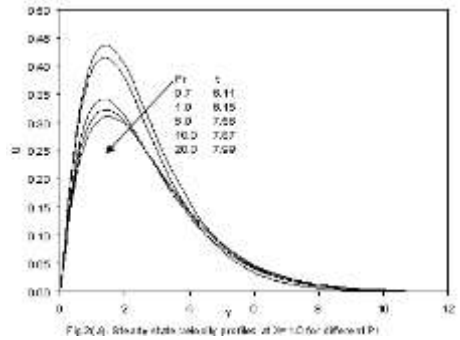

Fig.2(a). Steady state velocity profiles at X=1.0 for different Pr

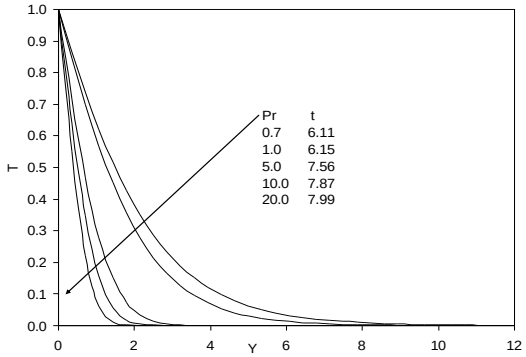

Fig.2(b). Steady state temperature profiles at X=1.0 for different Pr

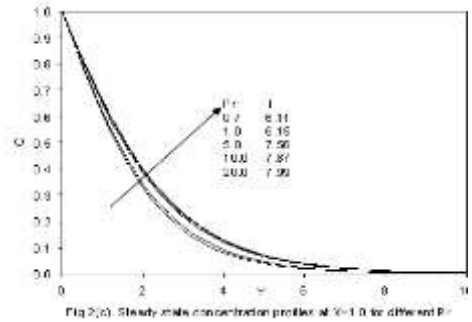

Fig.2(c). Steady state concentration profiles at X=1.0 for different Pr

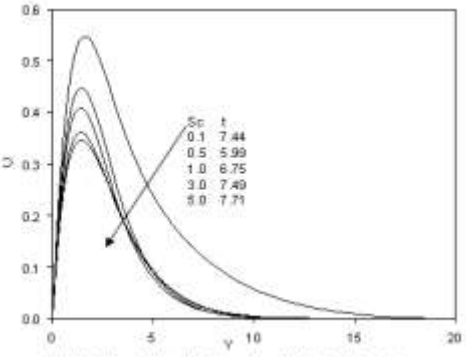

Fig.3(a). Steady state velocity profiles at X=1.0 for different Sc

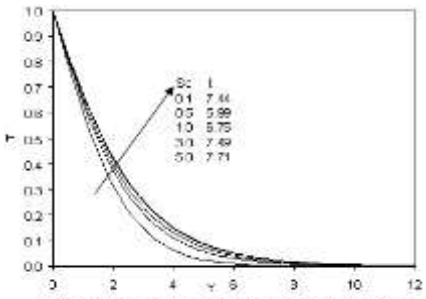

Fig.3(b). Steady state temperature profiles at X=1.0 for different Sc

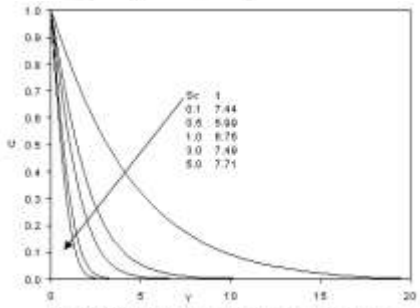

Fig.3(c). Steady state concentration profiles at X=1.0 for different Sc

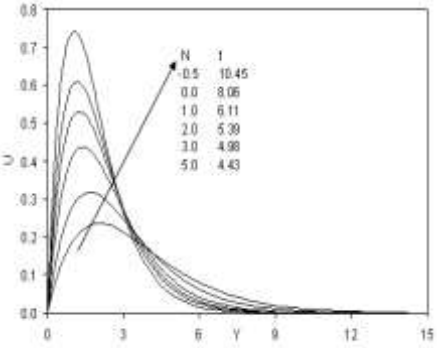

Fig.4(a). Steady state velocity profiles at X=1.0 for different N

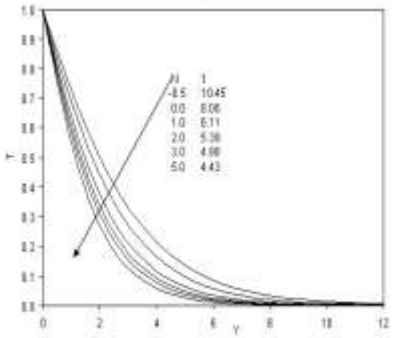

Fig.4(b).Steady state temperature profiles at X=1.0 for different N

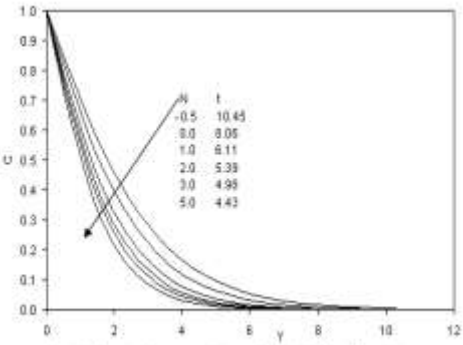

Fig.4(c). Steady state concentration profiles at X=1.0 for different N

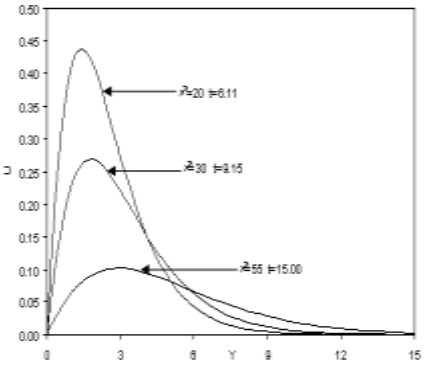

Fig.5(a). Steady state velocity profiles at X=1.0 for different m

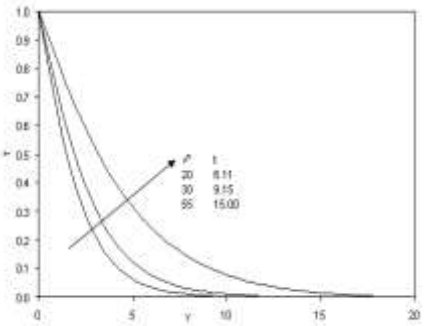

Fig.5(b). Steady state temperature profiles at X=1.0 for different m

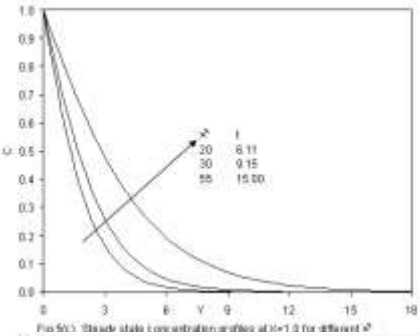

Fig.5(c). Steady state concentration profiles at X=1.0 for different m

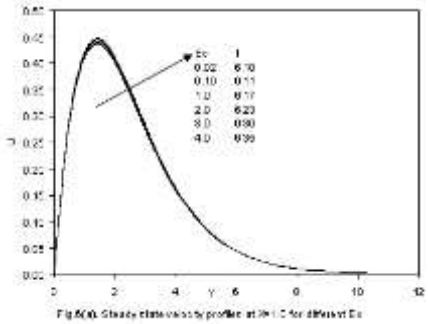

Fig.6(a). Steady state velocity profiles at X=1.0 for different Ec

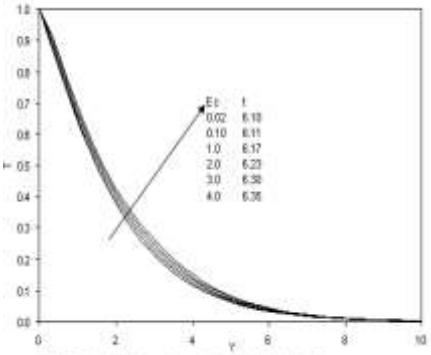

Fig.6(b). Steady state temperature profiles at X=1.0 for different Ec

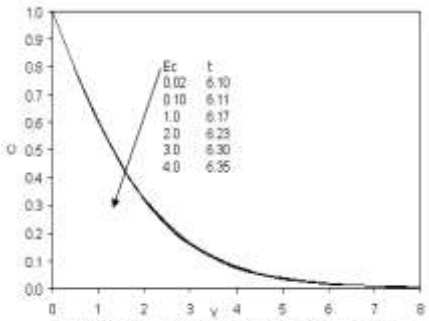

Fig.6(c). Steady state concentration profiles at X=1.0 for different Ec

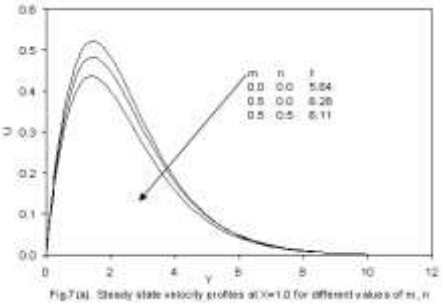

Fig.7 (a). Steady state velocity profiles at X=1.0 for different values of m, n

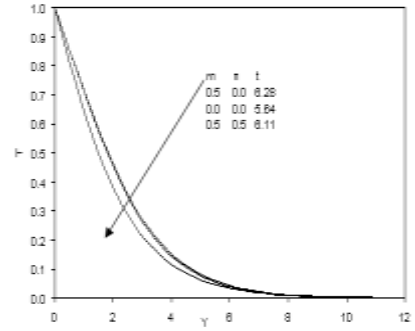

Fig.7(b). Steady state temperature profiles at X=1.0 for different m, n

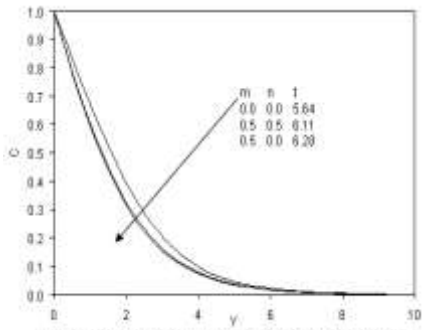

Fig.7(c). Steady state concentration profiles at X=1.0 for different m, n

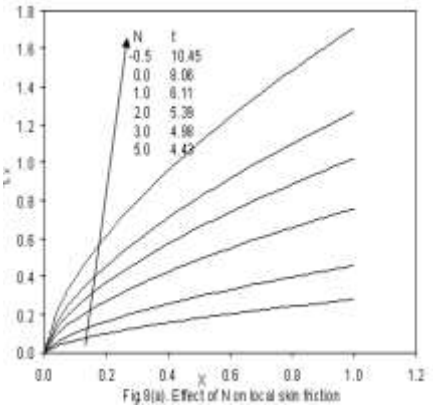

Fig.8(a). Effect of N on local skin friction

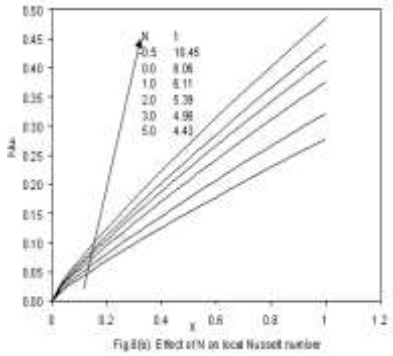

Fig.8(b). Effect of N on local Nusselt number

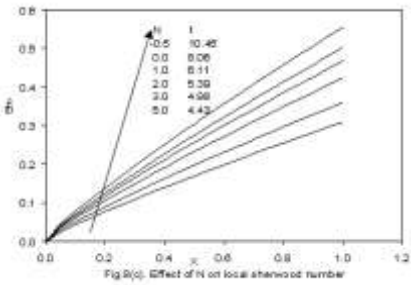

Fig.8(c). Effect of N on local sherwood number

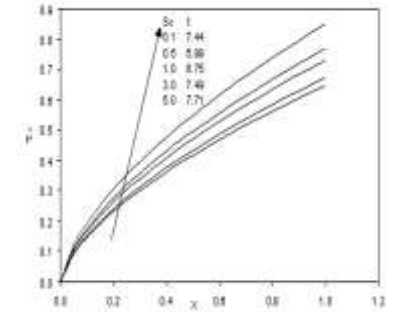

Fig.9(a). Effect of Sc on local skin friction

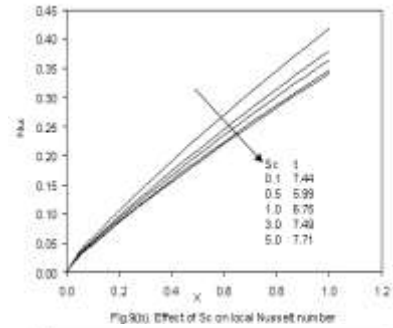

Fig.9(b). Effect of Sc on local Nusselt number

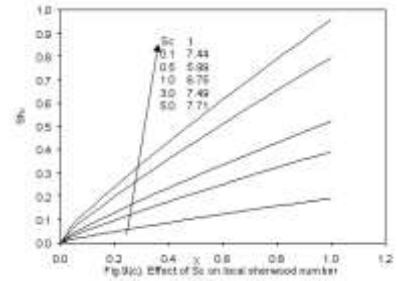

Fig.9(c). Effect of Sc on local sherwood number

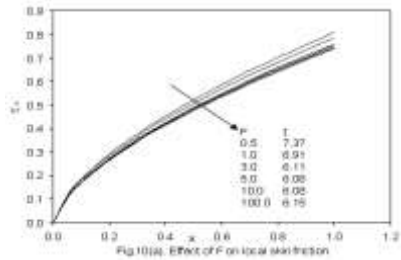

Fig.10(a). Effect of F on local skin friction

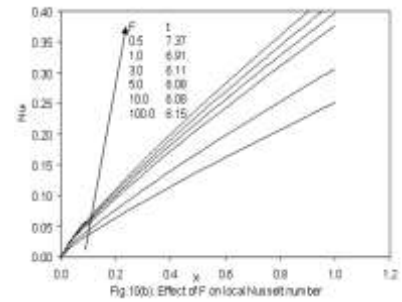

Fig.10(b): Effect of F on local Nusselt number

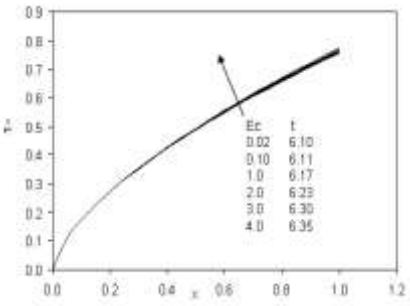

Fig.11(a): Effect of Ec on local skin friction

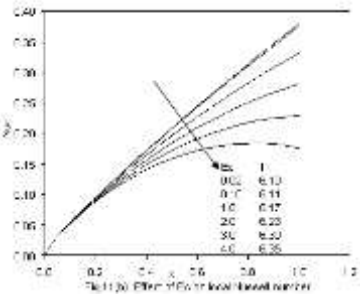

Since the present implicit Crank-Nicolson numerical difference code has been extensively validated against other numerical schemes by the authors [33, 18], it is extremely reliable and we omit comparison solutions with previous studies here for brevity. In figures 1a to 1c, the influence of radiation parameter, F on steady-state velocity, temperature and concentration distributions with distance transverse to the cone surface (i.e. with Y-coordinate) are shown. and this defines the ratio of thermal conduction contribution relative to thermal radiation. For radiative heat transfer dominance in the boundary layer regime, $F \to 0$.. For finite values of F there will be a simultaneous presence of thermal conduction and radiative transfer contributions. For $F = 1$ both modes will contribute equally. For $F \to \infty$, in equation (15), the term $4/3F \to 0$ and the energy conservation equation reduces to the conventional unsteady conduction-convection equation with dissipation i.e.

$$\frac{\partial T}{\partial t} + U\frac{\partial T}{\partial X} + V\frac{\partial T}{\partial Y} = \frac{1}{\Pr}\frac{\partial^2 T}{\partial Y^2} + Ec\left(\frac{\partial U}{\partial Y}\right)^2 \qquad (25)$$

An increase in F from 0 (total thermal radiation dominance) through 0.5, 1.0, 3.0, 5.0, 10.0 to 100.0, causes a significant decrease in velocity with distance into the boundary layer i.e. decelerates the flow. Velocities in all cases ascend from the cone surface, peak close to the wall and then decay smoothly to zero in the free stream. We also note that with increasing values of F the time taken to attain the steady state is reduced. Thermal radiation flux therefore has a de-stabilizing effect on the transient flow regime. This is important in polymeric and other industrial flow processes since it shows that the presence of thermal radiation while decreasing temperatures, will affect flow control from the cone surface into the boundary layer regime. As expected, temperature values are also significantly reduced with an increase in F as there is a progressive decrease in thermal radiation contribution accompanying this. All profiles are monotonic decays from the wall to the free stream. This trend concurs with the results of Bég et al [2], Chamkha et al [8] and Lin and Huang [26], all these studies also employing the Rosseland-diffusion approximation.

The maximum reduction in temperatures is witnessed relatively close to the cone surface since thermal conduction effects will be prominent closer to the cone surface, rather than further into the free stream. Concentration (C) is conversely boosted with an increase in F i.e. decrease in thermal radiation contribution. The parameter F does not arise in the species conservation equation (16) and therefore the concentration field is indirectly influenced by F via the coupling of the energy equation (15) with the momentum equation (16), the latter also being coupled with the convective acceleration terms in the species equation (16). However as with the response of the velocity and temperature fields, the increase in F decreases the time elapse to achieve the steady state. Therefore while greater thermal radiation augments diffusion of species in the regime it requires greater time to achieve the steady state.

In figures 2a to 2c, the spatial response of U, T and C profiles to Prandtl number (Pr) is illustrated. Pr defines the ratio of momentum diffusivity (□) to thermal diffusivity. It also expresses the ratio of the product of dynamic viscosity and specific heat capacity to the thermal conductivity of the principal fluid. Pr< 1 physically implies that heat will diffuse faster than momentum in the fluid. For Pr = 1 the diffusion rates will be the same for heat and momentum i.e. thermal and velocity boundary layer thicknesses will be equal. For Pr> 1 momentum will diffuse faster than heat. An increase in Pr from 0.7 (air) to 1, 5, 10 and the maximum value of 20, clearly decreases significantly streamwise velocity, U (figure 2a) for some considerable distance into the boundary layer. Flow is therefore decelerated with an increase in Prandtl number. At close proximity to the cone surface, velocities are all maximized for any value of Prandtl number, and then descend gradually to zero far from the cone surface. For increasing Pr values, the time, t, required to attain the steady state scenario is also elevated considerably. As such the steady state is achieved faster for gases than for lubricants and denser hydrocarbons (Pr> 5). Smaller Pr values will cause a thinner thermal boundary layer thickness and more uniform temperature distributions across the boundary layer. This is indeed observed in figure 2b, where with an increase in Pr the profiles descend increasingly more sharply from their maximum values at the cone surface (Y = 0) to zero. Smaller Pr fluids possess higher thermal conductivities so that heat can diffuse away from the cone surface (wall) faster than for higher Pr fluids (thicker boundary layers). With increasing Pr, once again the time taken to achieve the steady state is enhanced. The trend of these results agrees closely with other studies in the literature for example, Hasan and Mujumdar [20], Yih [39], Cheng [10] and Elperin and Fominykh [11] for the appropriate cases of Newtonian convective heat and mass transfer from a cone. As with the velocity and temperature distributions, the concentration profiles are computed at a location close to the leading edge of the boundary layer i.e. the cone apex (X = 0) , located at X = 1.0. Concentration is however enhanced with an increase in Prandtl number although the effect of Pr is much less pronounced in this case. The C profiles are more evenly distributed across the boundary layer. Increasing Pragain delays

the time taken, t, to achieve the steady state concentration distribution.

Figures 3a, b, c depict the variation of U, T, and C variables with Y-coordinate, for various Schmidt numbers (Sc). It is apparent from figure 3a, that with an increase in Sc, the time taken to attain the steady state does not follow a direct increase or decrease. For Sc= 0.1, t = 7.44 a value which decreases to 5.99 for Sc =.05 but then increases to 6.75 for Sc = 1.0 and then continues to increase to 7.49 for Sc = 3.0 and finally 7.71 for Sc = 5.0. The steady state is therefore achieved fastest for Sc = 0.5. With increasing Sc the velocity, U, is markedly depressed through the boundary layer i.e. the flow is retarded. We note that Sc = 0.1 is representative of hydrogen (low weight molecular gas) diffusing in air, Sc = 0.5 corresponds to oxygen diffusing in air, Sc = 1.0 to denser hydrocarbon derivatives as the diffusing species in air and Sc = 3.0 and 5.0 to increasingly higher molecular weight hydrocarbons. With lower Sc values the gradient of velocity profiles is greater prior to the peak velocity but lower after the peak i.e. the profiles decay more gradually to zero in the free-stream for Sc = 0.1 than for Sc> 0.1. Conversely with an increase in Sc, the temperature, T, as shown in figure 3b, increases continuously through the boundary layer. Again the steady state is attained fastest for Sc = 0.5 but slowest for Sc = 5.0. Figure 3c indicates that a rise in Sc strongly suppresses concentration levels in the boundary layer regime. All profiles decay monotonically from the cone surface (wall) to the free stream. Sc embodies the ratio of momentum diffusivity (□) to molecular diffusivity (D). For Sc> 1, momentum will diffuse faster than species causing progressively lower concentration values. For Sc< 1, species will diffuse much faster than momentum so that maximum concentrations will be generated in the boundary layer regime (Sc = 0.1). For lower Sc values there will be a more even distribution of concentration across the boundary layer. With a decrease in molecular diffusivity (rise in Sc) concentration boundary layer thickness is therefore decreased. For the special case of Sc = 1, the species diffuses at the same rate as momentum in the regime. For this scenario both concentration and velocity boundary layer thicknesses are the same. Higher Sc values will physically correspond to a decrease of molecular diffusivity (D) of the primary fluid causing a decrease in the rate of species diffusion. Lower Sc values will exert the reverse influence since they correspond to higher molecular diffusivities. Concentration boundary layer thickness is therefore considerably greater for Sc = 0.1 than for Sc= 5.

Figures 4a,b,c, present the effects of buoyancy ratio parameter, *N*, on U, T and C profiles. The maximum time elapse to the steady state scenario accompanies the only negative value of *N* i.e. *N* = -0.5. For *N* = 0 and then increasingly positive values of *N* up to 5.0, the time taken, *t*, is steadily reduced. As such the presence of *aiding* buoyancy forces (both thermal and species buoyancy force acting in unison) serves to stabilize the transient flow regime. The parameter $N = \frac{\beta^*(C'_w - C'_\infty)}{\beta(T'_w - T'_\infty)}$ and expresses the ratio of the species (mass diffusion) buoyancy force to the thermal (heat diffusion) buoyancy force. When *N* = 0 the species buoyancy term, *NC Cos* ϕ vanishes and the momentum boundary layer equation (14) is de-coupled from the species diffusion (concentration) boundary layer equation (16). Thermal buoyancy does not vanish in the momentum equation (16) since the term *T cos*ϕ is not affected by the buoyancy ratio. When *N*< 0 we have the case of opposing buoyancy. An increase in *N* from -0.5, through 0, 1, 2, 3, to 5 clearly accelerates the flow i.e. induces a strong escalation in streamwise velocity, *U*, close to the wall; thereafter velocities decay to zero in the free stream. At some distance from the cone surface, approximately *Y* = 3.1, there is a cross-over in profiles. Prior to this location the above trends are apparent. However after this point, increasingly positive *N* values in fact decelerate the flow. Therefore further from the cone surface, negative *N* i.e. opposing buoyancy is beneficial to the flow regime whereas closer to the cone surface it has a retarding effect. A much more consistent response to a change in the *N* parameter is observed in figure 4b, where with a rise from -0.5 through 0, 10.2.0, 3.0 to 5.0 (very strong aiding buoyancy case) the temperature throughout the boundary layer is strongly reduced. As with the velocity field (figure 4a), the time required to attain the steady state decreases substantially with a positive increase in *N*. Aiding (assisting) buoyancy therefore stabilizes the temperature distribution. A similar response is evident for the concentration distribution, *C*, which as shown in figure 4c, also decreases with positive increase in *N* but reaches the steady state progressively faster.

In figures 5a, b, c, the spanwise spatial distributions of the *U, T, C* variables with distance, *Y*, for various semi-apex cone angles, ϕ are presented. With wider cone angles i.e. a rise from 20 through 30 to 55 degrees (cone apex angle = 2ϕ =110 degrees), the flow is considerably decelerated in the near wall regime i.e. streamwise velocity profiles (*U*) are considerably reduced close to the cone surface. With further transverse locations from the wall into the boundary layer, however this trend is reversed and streamwise velocity, *U*, is marginally greater for wider cone apex angles than for smaller cone angles. With an increase in ϕ, there is a significant increase in the time elapsed to attain the steady state. In figure 5b, an increasingly wider cone apex angle induces greater temperatures continuously throughout the boundary layer i.e. heat the boundary layer regime. As for velocity profiles, an increase in ϕ causes much greater times required for the steady state to be achieved. In figure 5c, a similar response to the temperature field, is observed for the concentration field. *C* values are continuously enhanced with larger semi-apex cone angle. However although profiles all decay smoothly from the cone surface to the free stream, there is a faster descent in profiles than in the temperature field (figure 5b). Further from the wall, the influence of ϕ is considerably reduced for both temperature and concentration distributions.

Figures 6a, b, c illustrate the variation of *U, T, C* profiles with distance, *Y*, for various viscous dissipation parameter values i.e. Eckert number (*Ec*). Eckert number defines the ratio of the kinetic energy of the boundary layer flow to the enthalpy difference across the thermal boundary layer. *Ec*> 0 corresponds to cooling of the cone surface by convection currents. *Ec*< 0 corresponds to heating of the cone surface by convection currents. In these respective cases therefore heat is conducted away from the cone surface to the fluid and away from the fluid to the cone surface, respectively. In the present computations we have considered only the first of these cases.The dissipation effect arises in the energy equation (15) as the term, $Ec\left(\frac{\partial U}{\partial Y}\right)^2$ which couples the temperature field to the velocity field. This term is derived from the more general viscous heating effect term given in Gebhart [14]. Viscous dissipation is

approximately the difference between the total mechanical output by the stress system and the smaller quantity of total power input which produces thermodynamically reversible effects e.g. elevations in kinetic and potential energy. The discrepancy is the amount of energy dissipated as thermal energy. With a positive rise in *Ec*, there is a small increase in velocity close to the cone surface; however very close and further from the cone surface *Ec*exerts negligible influence on velocity profiles. With a strong rise in *Ec* from 0.02 through 0.1, 1.0, 2.0, 3.0 to 4.0, the time taken to attain the steady state is only slightly increased. There is a much more pronounced and consistent response in the temperature field, as shown in figure 6b. In consistency with the progressively greater conversion of mechanical energy into heat (and the fact that positive Ec corresponds to heat conduction from the cone surface to the external boundary layer flow regime), the temperature, *T*, in the boundary layer is elevated with a rise in *Ec*. Unlike the velocity response, the temperature profiles (*T*) are all monotonic decays from the cone surface. Again with an increase in *Ec* there is a small rise in the time, *t*, to achieve the steady state. Although the effect of increasing *Ec* is to again elevate the time taken to achieve the steady state, there is almost no distinguishable influence of a change in Eckert number on the concentration profiles, as shown in figure 6c. Viscous dissipation therefore does not affect noticeably the diffusion of species in the boundary layer.

In figures 7a,b,c, we have plotted the influence of the surface concentration power law exponent (*m*) and surface temperature power law exponent (*n*), on *U, C,T*, distributions with *Y* coordinate. For $m = 0$, the power-law variation of concentration reduces from $C' = C'_\infty + ax^m$ to $C' = C'_\infty + a$ i.e. we obtain an iso-species scenario (constant wall concentration). Similarly for $n = 0$ the power-law variation of temperature at the cone surface reduces from $T' = T'_\infty + ax^n$ to $T' = T'_\infty + a$ i.e. we obtain an isothermal scenario (constant wall temperature). For the doubly special case of $m = n = 0$, we observe in figure 7a that the velocity is maximized throughout the boundary layer. With an increase in *m* to 0.5 (non-iso-species case), but with isothermal wall characteristics ($n = 0$), the velocity is reduced in the boundary layer. For the doubly non-iso-species and non-isothermal case ($m = n = 0.5$) a further decrease is observed. As such increasing power-law exponents in the cone surface concentration and temperature variations serve to decelerate the flow in the boundary layer. For $m = n = 0$ the lowest time is achieved to arrive at the steady state. This value is increased for $m = 0.5$ and $n = 0$, but then reduced for $m = n = 0.5$, although in the latter case it is still greater than for the classic case of $m = n = 0$. Temperature response is somewhat different to an alteration in *m* and *n*. For $m = 0.5$ and $n = 0$, the temperature is maximized in the regime. For the double iso-thermal and iso-species case, i.e. for m = n = 0, there is a slight reduction in temperature further from the cone surface (Y = 0). However temperature is minimized for the doubly non-isothermal and non-iso-species case ($m = n = 0.5$), a trend sustained throughout the regime for all Y values. In the first of these *($m = 0.5, n = 0$)* cases the time needed to achieve the steady state is maximized; for *$m = n = 0$* it is minimized and then elevated for the *$m = n = 0.5$* case. Isothermal conditions therefore accelerate the arrival at the steady state whereas simultaneous non-iso-species and isothermal conditions delay this most. A similar pattern is computed for the concentration distributions in figure 7c, where exactly the same cases correspond to slowest and fastest attainment of steady state conditions. However in this case, concentrations are maximized for the double isothermal, iso-species case ($m = n = 0$), significantly reduced for the non-isothermal, non-iso-species case ($m = n = 0$) and then reduced further but only marginally for the non-iso-species, isothermal case ($m = 0.5$, $n = 0$). As with temperature profiles (figure 7b) a gradual descent in concentration profiles occurs from the wall (cone surface) to the free stream.

Figures 8a,b,c illustrate the shear stress (local skin friction), local Nusselt number and local Sherwood number distributions with streamwise coordinate for various buoyancy ratio parameters, N. A rise in N from negative to positive values, accompanying a stronger increase in assisted buoyancy, strongly accelerates the flow i.e. enhances shear stresses. The time required to attain the steady state is concomitantly decreased with this increase in N. Buoyancy-assisted flow therefore stabilizes the regime whereas buoyancy-opposing flow destabilizes the regime since the maximum time needed to reach steady state corresponds to N = -0.5. This concurs with earlier discussion relating to the flow velocity response to increasing N (figure 4a). Inspection of figures 8b and 8c shows that an increase in N strongly boosts both NuX and ShX i.e. enhances heat transfer gradient and mass transfer gradient at the cone surface. This trend is accentuated with further progression along the cone surface from the leading edge of the boundary layer (X = 0) to the furthest location downstream (X = 1.2). Simultaneously the time required to attain the steady state is reduced with an increase in N for both NuX and ShX.

Figures 9a,b,c depict the variation of cone surface shear stress (local skin friction), local Nusselt number and local Sherwood number distributions with streamwise coordinate for various Schmidt numbers (Sc). Increasing Sc clearly boosts the wall skin friction, □X which grows strongly from the leading edge downstream along the cone surface. The minimal time required to attain the steady state, as discussed earlier for concentration distributions, accompanies Sc = 0.5; the maximum time for reaching the steady state is associated with the maximum Schmidt number (Sc = 5, for which momentum diffusivity is five times the molecular diffusivity). Such results are important in chemical engineering process design since they indicate that lower molecular weight gases diffusing in air (e.g. Sc = 0.5 corresponds to oxygen) attain a steady state behaviour faster. With increasing Sc, local Nusselt number (figure 9b) is consistently reduced. Hence heat transfer rate at the cone surface is minimized for maximum Schmidt number (Sc = 5) and maximized for the lowest Schmidt number. The same characteristics for steady state behaviour as with the shear stress response (figure 9a) are observed for NuX variation in figure 9b. A much more dramatic response in ShX to an increase in Sc is observed in figure 9c. As expected surface species gradient i.e. mass transfer rate at the cone surface is strongly elevated with a rise in Sc and the profiles become increasingly divergent further downstream. Hence mass transfer rates are maximized further from the leading edge. Again the least time to attain the steady state arises for Sc = 0.5 and the greatest time for Sc = 5.0.

The effect of conduction-radiation parameter, F, oncone surface shear stress (□X), and local Nusselt number (NuX) variation are presented in figures 10a,b. With an increase in F, corresponding to progressively lower contributions of thermal radiation, wall shear stress is consistently reduced i.e. the flow is decelerated along the cone surface. However for each profile there is a growth in □X with distance from the leading edge (X

= 0 i.e. the cone apex) as we progress downstream. Increasing thermal radiation (i.e. decreasing F) acts to effectively accelerate the flow, concurring with the trend in figure 1a and the computations for flat plate [2] and also wedge [9] radiation–convection thermal boundary layers. Conversely however with greater thermal radiation (and lesser thermal conduction) contribution i.e. decreasing F values, the time required to attain the steady state is markedly increased. With an increase in F, local Nusselt number, NuX is considerably reduced; however for each profile NuX grows steadily in value with distance along the cone surface (X-coordinate). Heat transfer from the cone surface is therefore suppressed with increasing thermal radiation and enhanced with greater thermal conduction; also as before lower F values (stronger thermal radiation flux) necessitate greater times to reach the steady state.

Finally in figures 11a, b we have plotted the influence of Eckert number, *Ec* on the cone surface skin friction(τ_X), and local Nusselt number (Nu_X). As expected a very weak modification near the cone surface leading edge (X = 0) is experienced in τ_X profiles with a substantial increase in *Ec* from 0.02 to eventually 4.0, corresponding to a significant elevation in transport of heat from the cone surface to the fluid. The largest change is observed far downstream ($X \sim 1.0$) where a slight increase in shear stress accompanies the increment in *Ec* values i.e. there is asmall flow acceleration in this region. A small increase is also computed for the time taken to arrive at the steady state with an increase in *Ec*. In figure 11b a strong decrease in surface heat transfer rate is associated with an increase in Ec from 0.02 through 0.1, 1, 2, 3 to 4. With increasing *Ec* more and more thermal energy is transferred from the cone surface to the fluid so that simultaneously less and less heat is transferred to the cone surface from the external boundary layer regime. This results in a depression in cone surface heat transfer gradient (Nu_X). For low *Ec* values the Nu_X profiles are approximately linear growths; however with increasing *Ec* (2, 3, 4) the profiles become increasingly down-turned far downstream. For Nu_X = 4, the peak value is therefore near the end of the X-range rather than at the furthest location downstream as for *Ec* = 0.02, 0.1, 1, 2 and 3. As with the shear stress distributions, there is a small rise in time taken to arrive at the steady state with an increase in *Ec*.

Conclusions

A well-tested, stable, efficient Crank-Nicolson implicit finite difference procedure has been used to study numerically the transient free convective heat and mass transfer in boundary layer flow from a vertical cone with substantial thermal radiation and viscous heating effects. The computations have shown that increasing thermal radiation accelerates the flow, reduces temperature in the boundary layer and local Nusselt number but increases concentration values. An increase in viscous heating parameter as simulated via positive values of the Eckert number, causes very little change in velocity (principally near the cone surface) and shear stress distributions (principally far downstream from the leading edge) but considerably increases temperatures in the boundary layer, owing to the strong conversion of mechanical energy into thermal energy and conveyance of thermal energy from the cone surface to the fluid regime (wall cooling). A negative buoyancy ratio is found to decelerate the flow whereas the flow is considerably accelerated close to the wall with a positive increase in buoyancy ratio parameter, corresponding to the case where both thermal and species buoyancy forces assist each other in the regime. A positive increase in buoyancy ratio parameter is also found to markedly enhance local Nusselt number and local Sherwood number at the cone surface. The steady state response for the flow is also studied in detail. The present analysis has considered only the case of a Newtonian fluid and ignored thermal dispersion effects. The more complex case of a non-Newtonian flow with dispersion effects will be addressed in the near future.

References

[1]Banda M. K., Klar A and Seaïd M, A lattice-Boltzmann relaxation scheme for coupled convection-radiation systems, J. Computational Physics, 226(2007), 1408-1431.

[2]Bég, O.A. Takhar, H. S. Chamkha, A. J. Filip D. and Pop I. Mixed radiation-convection flow of an optically dense viscous fluid along a vertical surface in a non-Darcy geological porous system, Int. J. Applied Mechanics and Engineering, 8, 3(August 2003), 483-496.

[3]Bég, O. A. Zueco J.,Takhar H.S., Bég T.A., Sajid A,Transient nonlinear optically-thick radiative–convective double-diffusive boundary layers in a Darcian porous medium adjacent to an impulsively started surface: Network simulation solutions, Communications in Nonlinear Science and Numerical Simulation, 14, 11(2009),3856-3866.

[4]Bég O. A., Prasad V., Takhar H. S. andSoundalgekar V. M, Thermo-convective flow in an isotropic, homogeneous medium using Brinkman's vorticity model: Numerical study, Int. J. Numerical Methods in Heat and Fluid Flow, 8(1998), 59-89.

[5]Bég O.A., Bhargava R., Rawat S., Takhar. H.S. and Prasad, V.R, Numerical Study of heat transfer of a third grade viscoelastic fluid in non-Darcy porous media with thermophysical effects, PhysicaScripta, 77(2008), 1-11.

[6]Bég O.A., Bhargava R., Rawat S., Takhar. H.S. and K. Halim, Computational modeling of biomagneticmicropolar blood flow and heat transfer in a two dimensional non- Darcian porous medium, Meccanica, 43(2008), 391-410.

[7]Behnia, M. Reizes J. A. and De Vahl Davis G, Combined radiation and natural convection in a rectangular cavity with a transparent wall and containing a non-participating fluid, Int. J. Numerical Methods in Fluids, 10, 3(1990), 305-325.

[8]Carnahan B., Luther H. A., Wilkes J. O, Applied Numerical Methods, John Wiley & Sons, New York(1969).

[9]Chamkha, A. J, Takhar H. S, and Bég O. A., Radiative free convective non-Newtonian fluid flow past a wedge embedded in a porous medium, Int. J. Fluid Mechanics Research, 31(2004), 101–115.

[10]Cheng C-Y, Natural convection heat and mass transfer near a wavy cone with constant wall temperature and concentration in a porous medium, Mechanics Research Communications, 27 (2000), 613-620.

[11]Elperin, T. and Fominykh, A, Coupled mass and heat transfer between a cone and a power-law fluid, Chemical Engineering Technology , 27(2004), 757-762.

[12]EngelmanM.andJamnia M-A., Grey-body surface radiation coupled with conduction and convection for general geometries, Int. J. Numerical Methods in Fluids, 13, 8(1991), 1029-1053.

[13]Gebhart B, Buoyancy-Induced Flows and Transport, Hemisphere, Washington, USA, (1988).

[14]Gebhart, B, Effects of viscous dissipation in natural convection, Journal of Fluid Mechanics, 14(1962), 225-235.

[15]Gebhart, B. and Mollendorf, J, Viscous dissipation in external natural convection flows, Journal of Fluid Mechanics, 38(1969), 97-107.

[16]Gökoglu S.A. and Rosner D.E, Viscous dissipation effects on thermophoretically augmented aerosol particle transport across laminar boundary layers, Int. J. Heat and Fluid Flow, 6(1985), 293-297.
[17]Gorla, R. S. R. and Stratman, R. A, Natural convection boundary layer flow of water at 40C past slender cones, Int. Comm. Heat Mass Transfer, 13(1986), 403.
[18]GouseMohiddinS., Prasad V. R., Varma S. V. K. and Anwar Bég O, Numerical study of unsteady free convective heat and mass transfer in a Walters-B viscoelastic flow along a vertical cone, IMechE J. Mechanical Engineering Science, submitted June (2009)
[19]Hadley, G. R., Transparent boundary condition for the beam propagation method IEEE J. Quantum Electronics, 28(1992), 363-370.
[20]Hasan M. and Mujumdar A. S., Simultaneous heat and masstransfer in mixed convection along a vertical cone under uniform heat and uniform mass fluxes
Chemical Engineering Communications, 36(1985), 281- 298.
[21]Hassan H, Regnier N, and DefayeG., Effect of viscous dissipation on the temperature of the polymer during injection molding filling, Polymer Engineering and Science, 48(2008), 1199-1206.
[22]Hering, R. G. and Grosh. R. J, Laminar free convection from a non-isothermal cone, Int. J. Heat Mass Transfer, 5 (1962), 1059-1068.
[23]Keramida E. P., Liakos, H. H. Founti, M. A. Boudouvis A. G. and Markatos N. C, The discrete transfer radiation model in a natural gas-fired furnace, Int. J. Numerical Methods in Fluids, 34, 5(2000), 449-462.
[24]Krishnaprakas C.K., Narayana K.B. and Dutta P, Combined conduction and radiation heat transfer in a gray anisotropically scattering planar medium with diffuse-specular boundaries, Int. Comm. Heat and Mass Transfer, 28(2001), 77-86.
[25]Krýsa J., Houf, D. Oduoza C. F., Wragg A. A, Free convective mass transfer at up-pointing truncated cones, Chemical Engineering J., 85(2002), 147-151.
[26]Lin, J. D. and Huang, J. M., Radiation and convection in circular pipe with uniform wall heat flux, AIAA J. Thermophysics and Heat Transfer, 5(1991), 502-507.
[27]Mahajan, R. L. and Gebhart B. B, Viscous dissipation effects in buoyancy-induced flows, Int. J. Heat Mass Transfer, 32 (1989), 1380-1382.
[28]Mills, A. F., Convectiveheat and masstransfer to re-entry vehicles, Final Report School of Engineering and Applied Science, University of California at Los Angeles (UCLA), September(1978).
[29]Modest, M.F, Radiation Heat Transfer, MacGraw-Hill, New York, (1992).
[30]Moríñigo, J. A., Quesada, J. H., Analysis of viscous heating in a micro-rocket flow and performance, J. Thermal Science, 17, 2(2008), 116-124.
[31]MoriniG. L and Spiga, M, The role of the viscous dissipation in heated microchannels, ASME J. Heat Transfer, 129(2007), 308-318.
[32]Pop, I. and Takhar, H. S, Compressibility effects in laminar free convection from a vertical cone, Applied Scientific Research, A48(1991), 71-80.
[33]Prasad V. R., Bhaskar Reddy N and Muthucumaraswamy R, Radiation and mass transfer effects on two-dimensional flow past an impulsively started infinite vertical plate, Int. J. Thermal Sciences, 46, 12(2007), 1251-1258.
[34]Rajasekaran R and Palekar. M. G, Comparative effect of viscous dissipation on heat transfer in mixed convection flow: UWT and UHF cases, Astrophysics Space Science J., 106(1984), 73-80.
[35]Ransom J. B. and Fulton R. E, Concurrent implementation of the Crank-Nicolson method for heat transfer analysis, NASA Technical Memorandum 86448, Langley Research Center, Springfield, Virginia, USA(1985).
[36]Sayma A. I. and Betts P. L, Numerical modelling of thermal radiation absorption during the dispersion of dense gas clouds in the atmosphere, Int. J. Numerical Methods in Fluids, 26, 7(1998), 837-850.
[37]Takhar, H. S. Bég O. A. and Kumari M, Computational analysis of coupled radiation-convection dissipative non-gray gas flow in a non-Darcy porous medium using the Keller-Box implicit difference scheme, Int. J. Energy Research, 22(1998), 141–159.
[38]Weng, L.C. and Chu, H.S, Combined natural convection and radiation in a vertical annulus, Heat and Mass Transfer J., 31(1996), 371-379.
[39]Yih, K. A, Coupled heat and mass transfer by free convection over a truncated cone in porous media: VWT/VWC or VHF/VMF, ActaMechanica, 137(1999), 83-97.